Fractional dynamics and MDS visualization ofearthquake phenomena

AntónioM.Lopes, J.A.TenreiroMachado,C.M.A.Pinto,A.M.S.F.Galhano

ABSTRACT

This paper analyses earthquake data in the perspective of dynamical systems and frac- tional calculus (FC). This new standpoint uses Multidimensional Scaling (MDS) as a power- ful clustering and visualization tool. FC extends the concepts of integrals and derivatives to non-integer and complex orders. MDS is a technique that produces spatial or geometric representations of complex objects, such that those objects that are perceived to be similar in some sense are placed on the MDS maps forming clusters. In this study, over three mil- lion seismic occurrences, covering the period from January 1, 1904 up to March 14, 2012 are analysed. The events are characterized by their magnitude and spatiotemporal distri- butions and are divided into fifty groups, according to the Flinn–Engdahl (F–E) seismic re- gions of Earth. Several correlation indices are proposed to quantify the similarities among regions. MDS maps are proven as an intuitive and useful visual representation of the com- plex relationships that are present among seismic events, which may not be perceived on traditional geographic maps. Therefore, MDS constitutes a valid alternative to classic visu- alization tools for understanding the global behaviour of earthquakes.

Keywords:

1. Introduction

Earth's surface is made of several tectonic plates that move with respect to each other due to convection currents within the mantle below the terrestrial crust [1]. Neighbouring plates are separated by large fault zones and, when moving along the fault surfaces, exhibit friction and stick-slip behaviour [2–4]. Asperities between the plates may increase stress, leading to strain energy accumulation around the fault surface. Occasionally, when the stress is sufficiently high to break through the asperities, a sudden motion of the plates occurs, accompanied by energy release, causing an earthquake.

In certain models, the asperities on the fault surfaces are like fractals sliding over each other, explaining the fractal scaling behaviour that has been observed in earthquake phenomena [5]. Moreover, the tectonic plates form a complex system owing to interactions among faults [6–8]. An earthquake may not only release stress on the local fault, but also change stress conditions on other faults. Tectonic plate motion and strain accumulation processes interact on a range of scales from thousands of kilometres to millimetres and loading rates are not uniform in time [8,9]. Earthquakes reveal long-range correlations and long-memory characteristics [10], which are typical of fractional-order systems [11]. Complex correlations in space, time and magnitude are characterized by self-similarity and absence of characteristic length-scale, meaning that

seismic parameters exhibit power-law (PL) behaviour, as given by the Gutenberg–Richter (GR) and Omori laws [6,12]. The overall frequency distribution of earthquakes is given by the GR, which states that [13]

$$\log N(m) = q - r \cdot m \qquad (1)$$

where $N(m)$ is the frequency of earthquakes with magnitude greater than m, occurring in a specified area, r represents a parameter that has regional variation, being in the range $r \in [0.8; 1.06]$ for small and $r \in [1.23; 1.54]$ for big earthquakes, and q is a measure of the regional level of seismicity [14]. Given the relationship between seismic energy released and the magnitude of an earthquake, another form in which the GR law can be stated is:

$$N(\varepsilon) \approx \varepsilon^{-\tau} \qquad (2)$$

where $N(\varepsilon)$ is defined as previously but, in this case, for events which release energy greater than ε, and parameter $\tau \in [0.8; 1.05]$.

The (modified) Omori law describes the rate of decay of aftershock sequences, following a main event, and is formulated as [15]:

$$N(t) = C_1(t + C_2)^{-\alpha} \qquad (3)$$

where t is the time after the main shock, C_1 and C_2 are constants, and α is the rate of decay. For $\alpha = 1$ and $C_2 = 0$, the classical Omori law is obtained [16]. It was shown that values of α for aftershock sequences in Southern California vary in the interval $\alpha \in [0.5; 1.5]$, with mean value close to 1.0 [15,17]. The variability of α may be due to the tectonic conditions of the regions, but a significant factor controlling its value remains to be found [15]. The parameter C_1 is a measure of the aftershock productivity and is a function of the magnitude of the main event. The physical meaning of C_2 is involved in controversy. Some advocate that it relates to the physics of aftershock generation just after the main event, whereas others say that it models the incomplete detection of aftershocks at short times after the main earthquake. In [18] the authors use a pore pressure diffusion model and conclude that C_2 is dependent, at short times after the main earthquake, on the reducing process of high pore pressure gradients existing across a fault zone.

Earthquake phenomena have been studied in the perspective of complex systems and fractals. For example, in [19] a new model for earthquakes is proposed, given the observations of self-similarity in various length scales in the roughness of fractured solid surfaces. The authors demonstrate that the contact area distribution between two fractal surfaces follows a unique PL. In [20] the irregularity and complexity of earthquake ground motions is investigated from the perspective of nonlinear dynamics. Analysis based in chaotic dynamics theory and chaotic time series are suggested to examine the nonlinear dynamical characteristic of strong earthquake ground motions. The fractal geometry of various segments of the San Andreas Fault system was studied in [21], suggesting that differences between observed seismic activity might be attributed to differences in fault complexity and fractal dimensions. In [22] it is suggested that Self-Organized Criticality (SOC) is relevant for understanding earthquakes as a relaxation mechanism that organizes the terrestrial crust at both spatial and temporal levels.

In this paper, we analyse earthquake phenomena in the perspective of dynamical systems and fractional calculus (FC), using a new standpoint in this context. It is shown that the application of Fourier transforms and PL trendlines reveals fractional-order dynamics characteristics. Moreover, we show that earthquake's amplitudes follow a Beta distribution both at the regional and global levels. A large amount of data is analysed. The seismic events are divided into fifty groups, according to the Flinn–Engdahl (F–E) seismic regions, and correlation indices based on the Beta distribution parameters are proposed to quantify the similarities among regions. It should be noted that the indices used for MDS are not unique and are essentially determined by the user experience and intuition. Moreover, MDS has the advantage of avoiding sensitivity to the non-uniform spatial distribution of seismic events that result from poorly-instrumented areas.

FC refers to the branch of calculus that extends the concepts of integrals and derivatives to non-integer and complex orders [23–29]. In the past twenty years, FC emerged as an important tool for the study of dynamical systems, having ad–vantages where classical methods reveal strong limitations. Nowadays the application of FC concepts encompasses a wide spectrum of studies [30,31] such as, for example, dynamics of financial markets [32,33], biological systems [34,35], DNA sequencing [36], mechanical [37,38] and electrical systems [39,40], among others.

Previous work in the literature concerning application of MDS to earthquakes may be found in [41]. In this work, the authors used both multi-resolutional clustering and nonlinear MDS of earthquake patterns, in order to analyse synthetic and observed earthquake data. Observed seismic activity was related to Japanese islands between 1997 and 2003. They found that the combination of clustering results, in low- and high-resolution spaces, helped the recognition of precursory events more precisely than at a single resolution.

Bearing these ideas in mind, this paper is organized as follows. Section 2 describes the experimental dataset used in this study. Section 3 formulates the framework of the analysis of earthquake phenomena in the perspective of FC and investigates the fractional dynamics of the system. Section 4 introduces the MDS technique and the main concepts involved. Section 5 presents the application of the MDS method to earthquake data and discusses the results. Finally, Section 6 outlines the main conclusions.
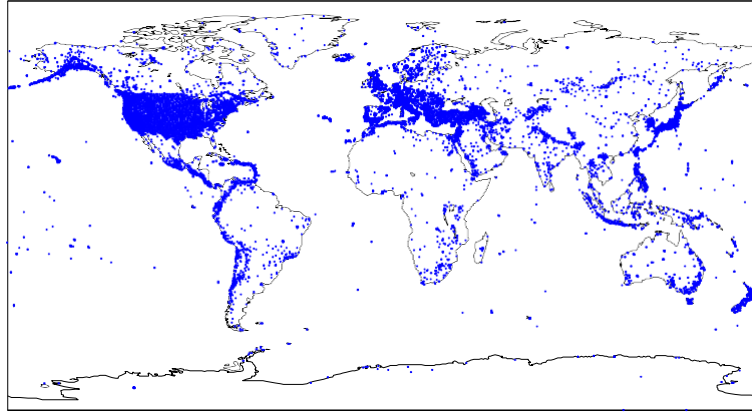
Fig. 1. Geographical location of the seismic stations (more than 17,000) that contributed to the ISC Bulletin.
Source: Data retrieved from http://www.isc.ac.uk/.
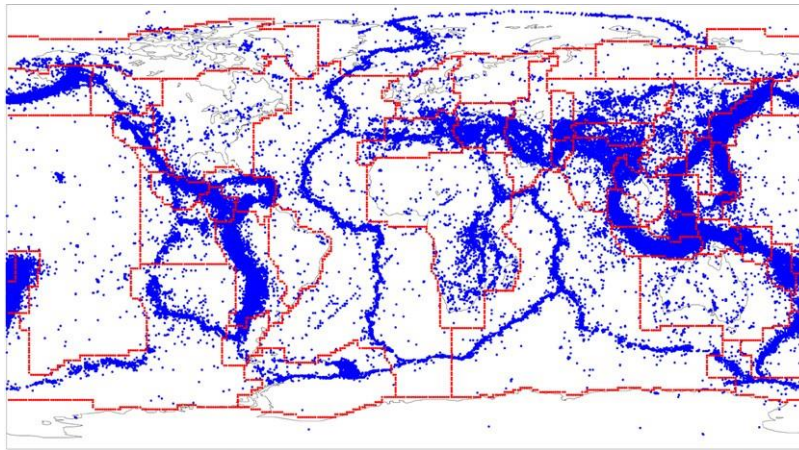
Fig. 2. Geographical location of seismic events, according to the ISC Bulletin (only the events with magnitude greater than four are depicted). The red lines represent the borders of the Flinn–Engdahl regions. The period of analysis is from 1904 up to April, 2012.

2. Brief description of the dataset

In this study the Bulletin of the International Seismological Centre (ISC), available online at http://www.isc.ac.uk/, is used [42]. The ISC Bulletin contains seismic events since 1904, relying on data contributed by seismological agencies from around the world. To date, a total of 487 agencies have contributed to the ISC Bulletin, reporting data collected by more than 17,000 seismic stations located worldwide (Fig. 1).

The data was retrieved in April, 2012. Each data record contains information about date and time, geographic location and magnitude of the events. As illustrated in Fig. 2, the seismic activity is far from being uniform across the Earth. In fact, the data reveals that most seismic activity occurs in three large zones [43]: (i) the Circum-Pacific belt (''Ring of Fire'') which extends from Chile, northward along the South American coast through Central America, Mexico, the West Coast of the United States, and the southern part of Alaska, through the Aleutian Islands to Japan, the Philippine Islands, New Guinea, the island groups of the Southwest Pacific, and to New Zealand (about 90% of the world's earthquakes occur in this zone); (ii) the second most seismic region (representing approximately 6% of all earthquakes) is the Alpide belt, that extends from the Mediterranean region, eastward through Turkey, Iran, and northern India; (iii) the third major region is the submerged mid-Atlantic Ridge.

Seismologists typically use seismic zones to localize earthquakes. The Flinn–Engdahl regionalization of Earth is the most used and consists in dividing Earth into fifty seismic regions, as shown in Fig. 2 [44–46]. Table 1 enumerates the F–E regions, the corresponding number of seismic events observed during the period of analyses and the maximum and minimum amplitudes registered.

Focusing on the magnitude of the events, the ISC Bulletin comprises occurrences in the interval $M_k \in [-2.1, 9.2]$, in a scale that is consistent with the local magnitude or Richter scale, which corresponds to the logarithm (in base ten) of the amplitude of the waves registered by seismographs. The distribution of the magnitudes of all world events in the database is

Table 1

Flinn–Engdahl regions and characterization of the data. The period of analysis is from 1904 up to April, 2012.

Region number	Region name	Number of seismic events	Minimum magnitude	Maximum magnitude
1	Alaska–Aleutian arc	39 196	1.2	8.3
2	Southeastern Alaska to Washington	19 650	0	8.1
3	Oregon, California and Nevada	26 801	0	8.2
4	Baja California and Gulf of California	7 711	0.5	7.5
5	Mexico–Guatemala area	30 294	0	8.1
6	Central America	20 671	0.9	7.8
7	Caribbean loop	48 932	0.3	8.1
8	Andean South America	81 766	0	8.6
9	Extreme South America	2 557	1.1	7.8
10	Southern Antilles	6 227	1.9	7.8
11	New Zealand region	58 759	0	8.1
12	Kermadec–Tonga–Samoa Basin area	50 764	0.7	8.3
13	Fiji Islands area	23 957	1.2	7.9
14	Vanuatu Islands	29 477	0	8.2
15	Bismarck and Solomon Islands	29 895	0.3	8.1
16	New Guinea	25 221	−0.1	7.9
17	Caroline Islands area	5 097	1.7	7.9
18	Guam to Japan	34 335	1	8.1
19	Japan–Kuril Islands–Kamchatka Peninsula	867 008	−1.4	8.5
20	Southwestern Japan and Ryukyu Islands	584 156	−1.4	8.2
21	Taiwan area	286 413	−0.2	8
22	Philippine Islands	31 723	0	8.4
23	Borneo–Sulawesi	34 807	1.2	8.2
24	Sunda arc	47 076	0	8.4
25	Myanmar and Southeast Asia	8 327	0.1	8
26	India–Xizang–Sichuan–Yunnan	32 256	−0.8	8.6
27	Southern Xinjiang to Gansu	17 563	0	8.5
28	Lake Issyk-Kul to Lake Baykal	34 596	0	8.4
29	Western Asia	22 092	0	8.2
30	Middle East-Crimea–Eastern Balkans	223 922	0	8.4
31	Western Mediterranean area	195 228	−0.6	7.5
32	Atlantic Ocean	37 849	0	8.3
33	Indian Ocean	13 175	1.3	7.9
34	Eastern North America	15 258	0	7.8
35	Eastern South America	68	3.1	5.7
36	Northwestern Europe	92 045	−0.5	6.3
37	Africa	49 498	−0.3	7.4
38	Australia	7 813	0	7.8
39	Pacific Basin	3 040	−2.1	7.2
40	Arctic zone	18 993	0	7.1
41	Eastern Asia	15 423	0	7.8
42	Northeast. Asia, North. Alaska to Greenland	6 941	0	7.6
43	Southeastern and Antarctic Pacific Ocean	7 076	2.2	7.1
44	Galápagos Islands area	2 402	2.3	6.8
45	Macquarie loop	1 792	2.1	7.8
46	Andaman Islands to Sumatera	21 038	0.6	9.2
47	Baluchistan	4 155	1.8	7.6
48	Hindu Kush and Pamir area	41 023	0	8
49	Northern Eurasia	60 156	−0.6	6.8
50	Antarctica	68	2.2	5.5

depicted in Fig. 3 and compared to both the Gaussian and Beta distributions. While the Gaussian $y = a \cdot \exp[-(x-b)^2/(2c)^2]$, with $a = 0.0287$, $b = 2.0320$ and $c = 1.4265$, represents a rough approximation ($R^2 = 0.97$), the results show that the Beta distribution $y = a(x - b)^c \cdot (x - d)^e$, with $a = 0$, $b = -1.4819$, $c = 3.7811$, $d = 12.2374$ and $e = 12.0274$, fits more adequately the data ($R^2 = 0.99$). On a regional basis (i.e., analysing the events according to the F–E regions) an identical behaviour is observed and discussed in Section 4 in combination with the MDS analysis.

3. Fractional dynamics in earthquake phenomena

In this section earthquake phenomena are analysed in the perspective of complex systems that react to stimuli and the corresponding response signals are studied by means of the Fourier transform. The seismic events are divided into fifty groups, according to the F–H regions where they took place. The events belonging to F–E region i ($i = 1, \ldots, 50$) are represented by:

$$x_{FE_i}(t) = \sum_{k=1}^{T} M_k \delta(t - t_k) \tag{4}$$
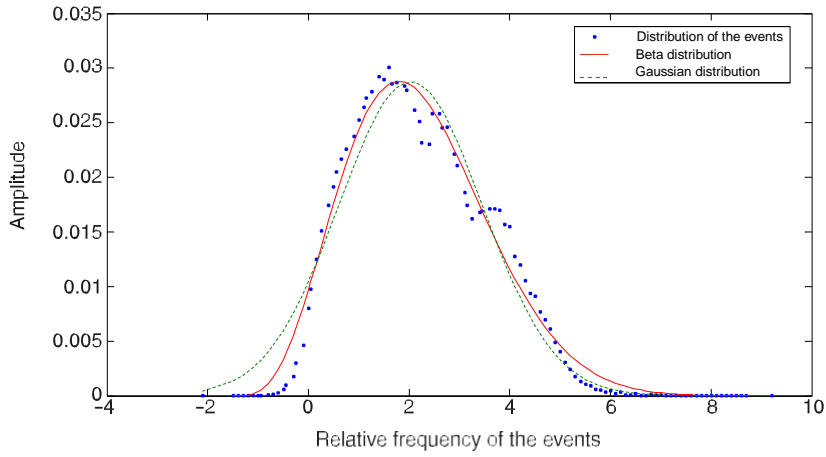
Fig. 3. Distribution of the magnitudes of the ISC seismic events: (a) comparison to the Gaussian distribution $y = a \cdot \exp[-(x-b)^2/(2c)^2]$ ($R^2 = 0.97$); (b) comparison to the Beta distribution $y = a(x-b)^c \cdot (x-d)^e$ ($R^2 = 0.99$).
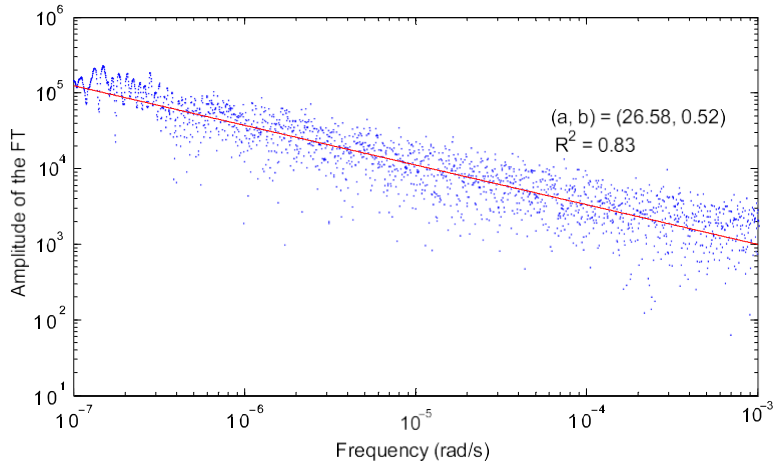
Fig. 4. Magnitude of the FT of the signal $x_{FE_{19}}(t)$, which represents the seismic activity in the F–E region number 19, and the corresponding PL approximation.

meaning that the seismic events are modelled as Dirac impulses, $M_k \delta(t - t_k)$, where M_k represents the magnitude, t_k is the time of occurrence, parameter t represents time and T is the total time period of study, both expressed in seconds [47]. Hence, each $x_{FE_i}(t)$ is a time-domain signal that corresponds to the sequence of all seismic events, registered in every F–E region, over the time of study. In our methodology $x_{FE_i}(t)$ are representative signals of the earthquake dynamics. Processing these time-domain signals with the Fourier transform and, given the characteristics of the resulting spectrum, approximating the amplitude by means of a power functions, will reveal dynamical characteristics of the system.

In analytical terms, for the signal $x_{FE_i}(t)$, we have:

$$F\left\{x_{FE_i}(t)\right\} = X_{FE_i}(j\omega) = \int_{-\infty}^{+\infty} x_{FE_i}(t) \cdot e^{-j\omega t} \cdot dt \qquad (5)$$

where F represents the Fourier operator, ω denotes the angular frequency and $j = \sqrt{-1}$.

Fig. 4 illustrates a typical spectrum, namely the spectrum of $x_{FE_{19}}(t)$, corresponding to the F–E region number 19 (Southwestern Japan and Ryukyu Islands). As can be seen, a PL approximation, given by

$$\left|F\left\{x_{FE_i}(t)\right\}\right| = \left|X_{FE_i}(j\omega)\right| \approx a \cdot \omega^{-b}, \quad a \in \Re^+, \ b \in \Re \qquad (6)$$

fits the spectrum well, revealing characteristics that are usually found in fractional-order dynamic systems [48,49]. For this case, we obtain the parameters $(a, b) = (26.58, 0.52)$, computed by a least squares fitting procedure, leading to a fractional value of parameter b.

In the following the parameters (a, b) were computed for all signals $x_{FE_i}(t)$ ($i = 1, \ldots, 50$). Fig. 5 represents the map of $\log(b)$ versus $\log(a)$, showing that there exists a strong correlation between the two parameters. The area of the bubbles on the graph is proportional to the reciprocal of the coefficient of determination of each PL fit.
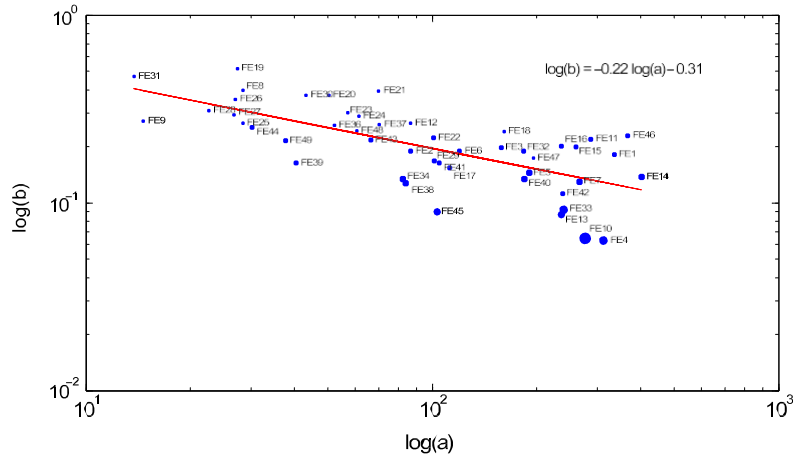
Fig. 5. Mapping of $\log(b)$ versus $\log(a)$ and the corresponding PL parameters (0.49, 0.22).

It can be seen that a straight line fits quite well into the data, meaning that in loglog scales (b, a) approximately follow a PL with parameters (0.49, 0.22). This means that using the two parameters is somewhat 'redundant', and parameter b is sufficient to characterize earthquake phenomena. Moreover, we verify that $b \in [0; 1]$, which can be viewed as the cases of white and pink noises, respectively.

4. Multidimensional scaling techniques

MDS is a set of techniques that produce spatial or geometric representations of complex objects. It helps in understanding people's judgements (preference, relatedness) concerning elements in sets of objects [50]. Each object is represented as a point in an m-dimensional space. MDS uses proximity measures in high-dimensional space to build a new geometrical configuration of points. This configuration preserves the proximities of the high-dimensional space, and eases the understanding of data underlying the structure. MDS is, consequently, different from other similar techniques, such as factor analysis and cluster analysis, because there are no assumptions concerning which factors might drive each dimension. Additionally, MDS algorithms have better convergence rates than other algorithms and are less complex [51]. MDS treats every type of data, negative, non-negative, correlations, amongst others [52].

The proximity measures the (dis)similarities among the items and is, usually, a distance measure. Smaller (larger) distances between two objects translate into more (less) similarities between them. Let n be the number of different objects and let the dissimilarity for objects i and j be given by δ_{ij}. The coordinates are gathered in an $n \times q$ matrix **X**, where q is the dimensionality of the solution (to be specified in advance by the user). Thus, row i from **X** gives the coordinates of object i. For example, the Minkowski distance metric provides a general way to specify distance for quantitative data in a multidimensional space:

$$d_{ij} = \left(\sum_{k=1}^{q} w_k |x_{ik} - x_{jk}|^r \right)^{1/r} \tag{7}$$

where x_{ik} and x_{jk} are the values of the i-th and j-th objects at k-dimension, W_k is a weighting factor and $r > 0$ is a parameter. Often all k components are treated identically and $W_k = 1$ is adopted. For $r = 1$, $r = 2$ and $r \to \infty$ we get the Manhattan, Euclidean and Chebyshev distances, respectively.

Nevertheless, the MDS technique allows users to choose any metric for comparing objects, which leads to a rich pool of possibilities.

The main purpose of MDS is to find a matrix **X** such that d_{ij} approximates δ_{ij} as closely as possible. Mathematically, this problem is equivalent to minimizing the raw Stress function, σ^2, given by [53]:

$$\sigma^2 = \sum_{i=2}^{n} \sum_{j=1}^{i-1} z_{ij} (\delta_{ij} - d_{ij})^2 \tag{8}$$

where z_{ij} is a nonnegative weight chosen by the user. Usually, a value of $z_{ij} = 0$ means that dissimilarities are absent. MDS uses numerical algorithms to find matrices **X** for which σ^2 is a minimum. There are other stress measures, such as the normalized raw Stress, which is σ^2 divided by the sum of squared dissimilarities.

Other measures are Kruskal's Stress-1 and Kruskal's Stress-2, which divide σ by the sum of squared distances or by a function of the variances of distances, respectively. Another example is the S-Stress measure, given by the sum of squared errors between squared distances and squared dissimilarities.
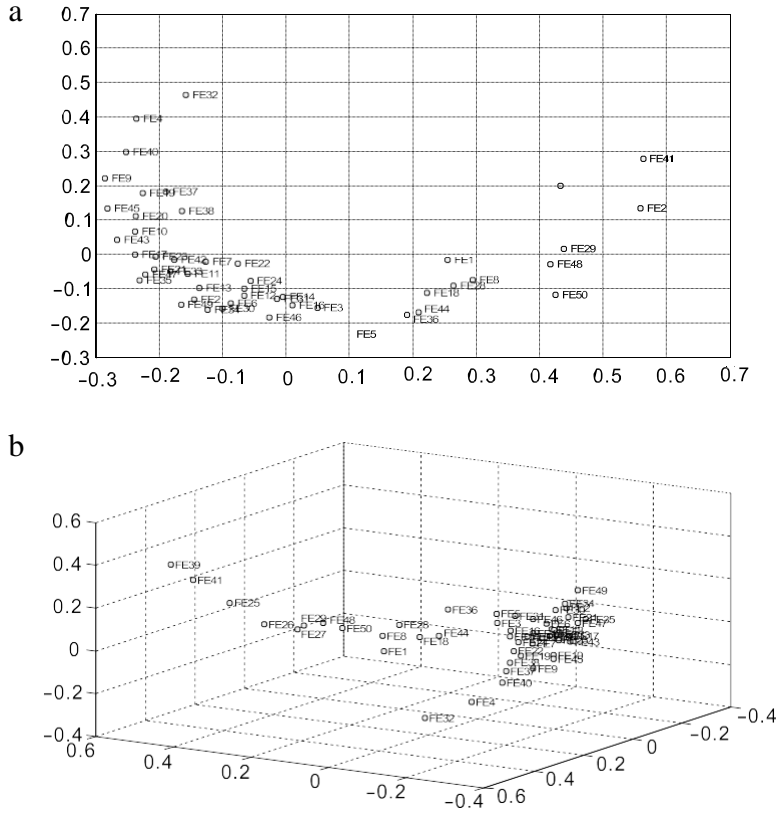
Fig. 6. MDS maps: (a) 2D; (b) 3D. The cosine correlation index d_{ij}^c is used. Each point represents a F–H region.

The Shepard diagram can be used to infer the quality of the MDS solution. Let p_{ij} denote the similarities between objects i and j. A Shepard diagram consists of pairs (p_{ij}, d_{ik}), (p_{ij}, δ_{ik}). A line is drawn connecting the pairs (p_{ij}, δ_{ik}). The approximation error, concerning dissimilarities of each object, is given by $d_{ij} - \delta_{ij}$. The Shepard diagram is thus useful to visualize the residuals and outliers resulting from the MDS application to the data.

MDS can be divided according to the classification of data similarities, number of similarity matrices and the nature of the MDS model. We thus have a non-metric MDS, if similarity data are qualitative, and a metric MDS for quantitative similarities. As regards the number of similarity matrices and the nature of the model, there are several MDS types. Classical MDS has one matrix and unweighted models, replicated MDS deals with several matrices and unweighted models, and finally weighted MDS has several matrices and weighted models.

Usually, MDS geometric visualizations are performed in two or three dimensions; nevertheless, any dimension q, with $q < m$ is possible.

MDS has been used on a large variety of real data, such as finance, marketing, sociology, physics, political science, biology and biomedics [54–59]. Other relevant research areas, such as for wireless network sensors, are also becoming interested in MDS analysis [60,61].

To conclude this brief review in MDS techniques, we emphasize that some caution must be taken when analysing MDS maps. One must take into account that the axes of the maps are meaningless, the orientation of the geometrical configuration is arbitrary, and the substantive dimensions or attributes under analysis do not need to correspond in number or direction to the mathematical dimensions (axes) which define the vector space. The latter is explained by the fact that mathematical and human dimensions are different. Mathematical dimensions are orthogonal, by definition, whereas human dimensions may have a highly degree of correlation.

5. MDS analysis of earthquake phenomena

In this section, we use the MDS technique to compare the $n = 50$ F–E regions. Firstly, the distributions of amplitudes of the events in every F–E region are approximated by means of Beta distributions. The corresponding parameters, $\beta_{FE_j} = \{a_j \ b_j \ c_j \ d_j \ e_j\}$, $(j = 1, \ldots, n)$, characterize those regions. Two indices are proposed to quantify the similarities among seismic regions and the MDS maps generated and analysed. In this line of thought, in Section 5.1, the cosine correlation index is considered and, in Section 5.2 we use the Euclidean distance correlation index.
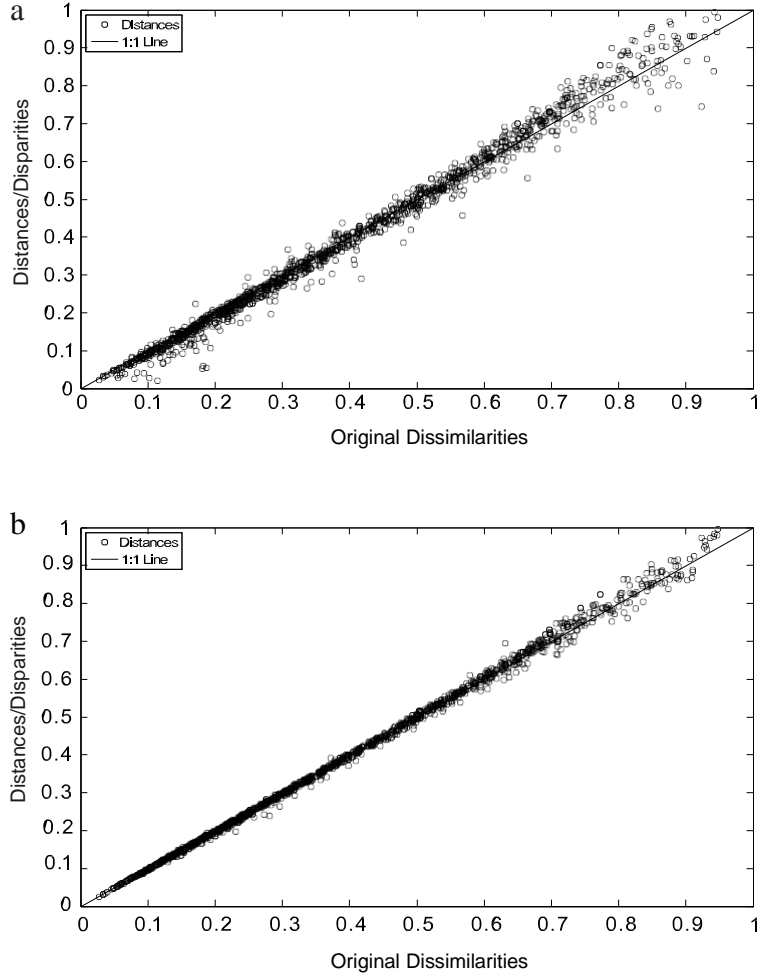
Fig. 7. Shepard plots: (a) 2D; (b) 3D. The cosine correlation index d^c_{ij} is used.

### 5.1. MDS analysis based on cosine correlation index

The cosine correlation index, d^c_{if} defined by Eq. (9), is considered for construction of matrix X.

$$d^c_{ij} = \left(\frac{\sum\limits_{p=1}^{nP} \beta_{FE_i}(p) \cdot \beta_{FE_j}(p)}{\sqrt{\sum\limits_{p=1}^{nP} \beta^2_{FE_i}(p) \cdot \sum\limits_{p=1}^{nP} \beta^2_{FE_j}(p)}} \right)^2 \qquad (9)$$

where the vectors $\beta_{FE_i}(p)$ and $\beta_{FE_j}(p)$ represent every $(i,\ j)$ F–E regions and $nP = 5$ is the total number of parameters of the Beta distributions. Based on this index, an $n \times n$ symmetric matrix, **C**, is computed and, in order to reveal possible relationships between the F–E regions under analysis, the MDS technique is used. In this perspective, while several MDS criteria were tested, the Sammon criterion revealed good results and was adopted in all simulations. It should be noted that this criterion tries to optimize a cost function that describes how well the pairwise distances in a data set are preserved [62,63].

Fig. 6 depicts the 2D and 3D locus of the F–E regions given by the MDS. Each point on the map represents a region. We can notice that (i) one main cluster groups the majority of the regions; two smaller 'central' clusters comprise, respectively, the regions (ii) {FE1, FE8, FE18, FE28, FE36, FE44} and (iii) {FE26, FE27, FE29, FE48, FE50}, the latter farther away from the main cluster; the regions (iv) FE25, FE41 and FE39 tend to be farther away from the main cluster, on one side, and also the regions (v) FE4 and FE32, on the other side. Therefore, cases (iv) and (v) can be interpreted as being quite different from the rest (and from each other), in the perspective of the cosine correlation index (9).
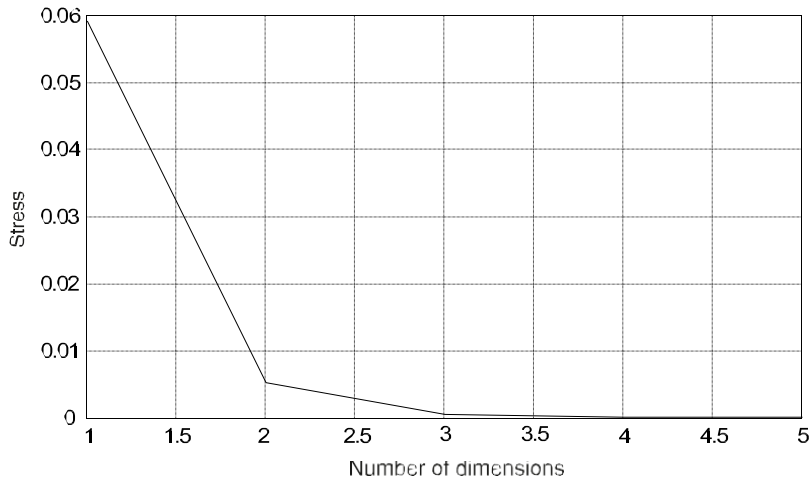
Fig. 8. Stress plot. The cosine correlation index d_{ij}^c is used.
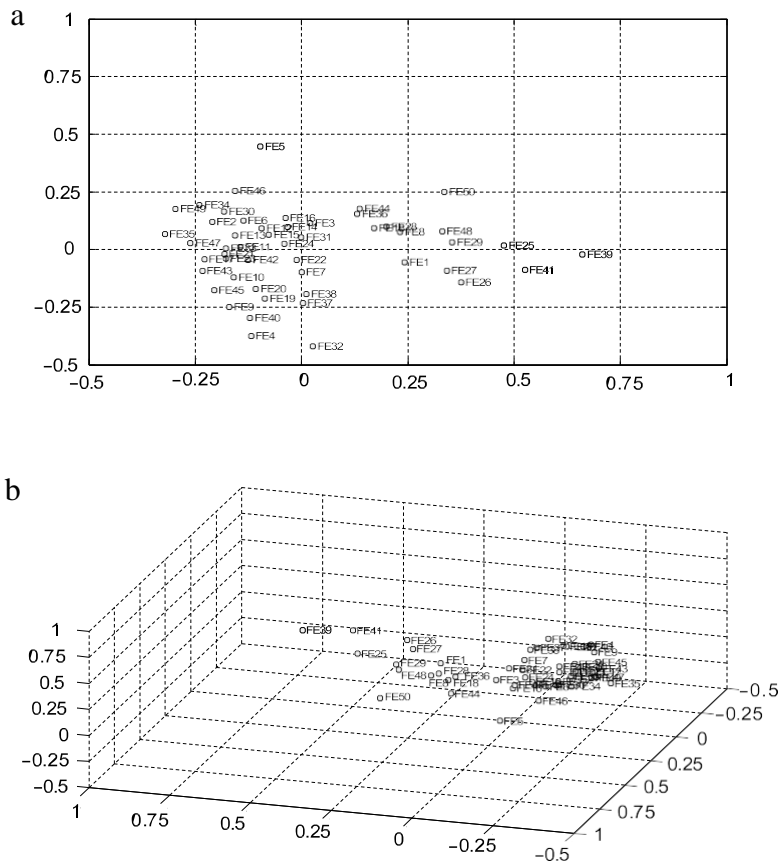
Fig. 9. MDS maps: (a) 2D; (b) 3D. The frequency-domain correlation d_{ij}^e is used. Each point represents a F–H region.

We should note that MDS is merely a mathematical visualization tool and that a physical perspective of the reported results must be found in the light of the measuring index. Therefore, a further explanation about physical mechanisms associated with the results must be envisaged by standard complementary procedures.

Figs. 7 and 8 depict the Shepard and stress plots, respectively. The Shepard diagram shows a reasonable distribution of points around the 45° line, particularly when the dimensionality is three, which means a good fit of the distances to the dissimilarities. The stress plot reveals that a three-dimensional space describes well the locus of the fifty F–E regions. In fact, the stress diminishes strongly until the dimensionality is two, moderately towards dimensionality three and weakly from
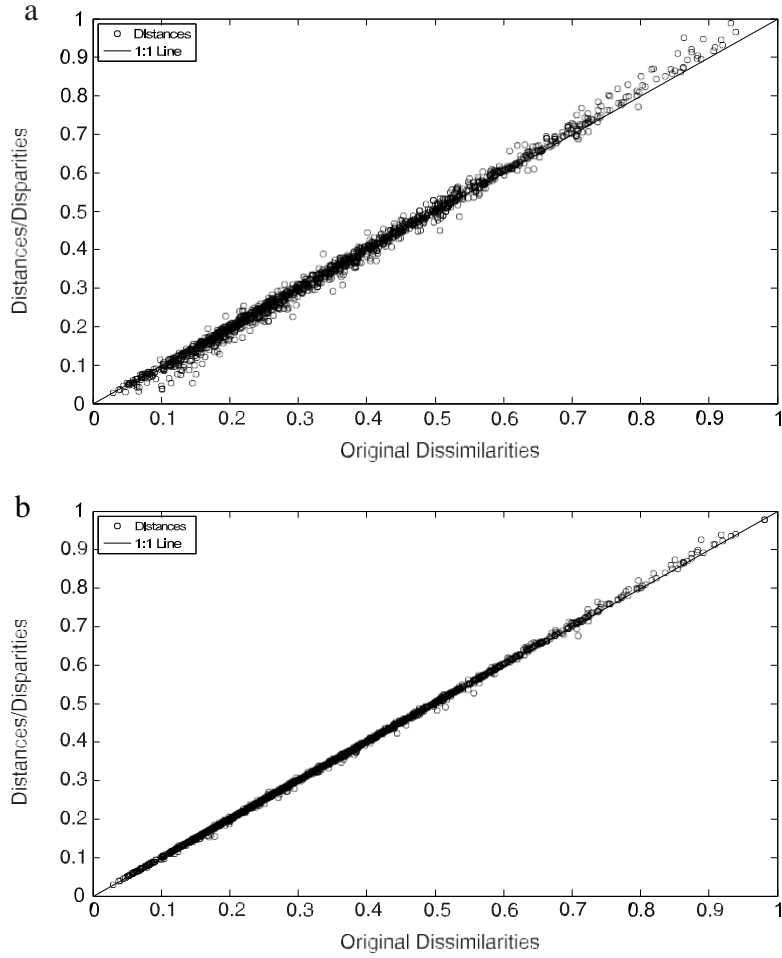
Fig. 10. Shepard plots: (a) 2D; (b) 3D. The frequency-domain correlation d^e_{ij} is used.

then on. The maximum curvature point of the stress plot is often adopted as the criterion for deciding the dimensionality of the MDS maps. This means that, although four or five dimensions would represent the data more accurately, 3D maps are a good compromise between accuracy and easiness of visualization.

5.2. MDS analysis based on Euclidean distance correlation index

In this subsection we consider a second index for construction of matrix X. Adopting now the methodology established in Section 5.1, a new correlation index based on the Euclidean distance is tested. Mathematically, this index, d^e_{ij} is defined by expressions (10) and (11):

$$d_{ij} = \sum_{p=1}^{nP} \left(\beta_i(p) - \beta_j(p) \right)^2 \tag{10}$$

$$d^e_{ij} = 1 - \frac{d_{ij}}{\max(d_{ij})}. \tag{11}$$

The 2D and 3D locus of the F–E regions resulting from the MDS analysis are represented in Fig. 9, which suggests that: (i) the regions are organized on the MDS map forming two main clusters, one being much larger than the other; (ii) similarly to the results shown before, regions FE25, FE41 and FE39 are located on the border of one cluster; (iii) as also are regions FE4 and FE32.

We observe now a different pattern or, in other words, a distinct ''shape'', but the main idea of clustering remains. This observation is usual in MDS plots, where alternative indices, capturing different characteristics of the phenomena, lead to unidentical plots, but revealing the same type of conclusion.
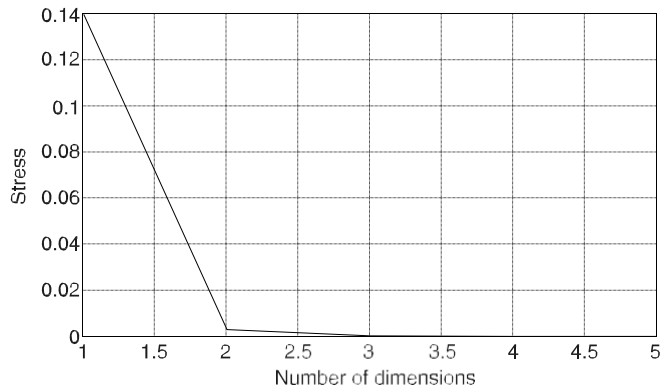
Fig. 11. Stress plot. The frequency-domain correlation d_{ij}^e is used.

The Shepard plots depicted in Fig. 10 reveal a good distribution of points around the 45° line. This distribution is even better than the one obtained for the time-domain correlation index, especially for the 3D maps. The stress plot (Fig. 11) shows that a three-dimensional space describes well the locus of the regions and, again, that d_{ij}^e gives results more accurate than d_{ij}^c.

In conclusion, both correlation indices proved to be adequate for representing the similarities between seismic regions. The adopted indices are not unique and different indices lead to different charts. These charts can be ''better'' or ''worse'' in the sense of getting a clear visualization. Usually, for different MDS plots (from distinct indices) conclusions are similar, but there is no ''theorem'' that proves that. Therefore, the choice of one of the alternative indices as the ''best'', or even the definition of another index, is not a matter of being correct or wrong. The choice of the ''adequate'' index for MDS construction is strictly based on the user experience and intuition, this issue remaining to be further explored.

6. Conclusion

Fractional calculus tools and Multidimensional Scaling analysis was proposed to characterize the dynamics and visualize the similarities among Earth's seismic regions. The Flinn–Engdahl (F–E) regionalization was adopted in this study. The Bulletin of the International Seismological Centre, available online at http://www.isc.ac.uk/, was used. The dataset covers the period from 1904 up to the present date, relying on more than three million events from around the world. Two correlation indices were used to quantify the similarities between regions. MDS maps were proved to be an intuitive and useful visual representation of the complex relationships that are present among seismic events, which are not perceived on traditional maps. The dynamics of earthquakes is complex and difficult to model. Furthermore, real data has an unstructured spatial distribution caused by the existence of geographic areas with a reduced instrumentation. However, MDS constitutes a valid alternative to analyse the available data, while avoiding modelling exercises that can lead to imprecise conclusions. This paper demonstrates the feasibility of the proposed method and encourages further research taking into account present day visualization techniques.

References

[1] G. Stadler, M. Gurnis, C. Burstedde, L.C. Wilcox, L. Alisic, O. Ghattas, The dynamics of plate tectonics and mantle flow: from local to global scales, Science 329 (2010) 1033–1038.
[2] P. Bhattacharya, B. Chakrabarti, Kamal, A fractal model of earthquake occurrence: theory, simulations and comparisons with the aftershock data, J. Phys. Conf. Ser. 319 (2011) 012004.
[3] J.M. Carlson, J.S. Langer, B.E. Shaw, Dynamics of earthquake faults, Rev. Modern Phys. 66 (1994) 657–670.
[4] V. De Rubeis, R. Hallgass, V. Loreto, G. Paladin, L. Pietronero, P. Tosi, Self affine asperity model for earthquakes, Phys. Rev. Lett. 76 (1996) 2599–2602.
[5] R. Hallgass, V. Loreto, O. Mazzella, G. Paladin, L. Pietronero, Earthquake statistics and fractal faults, Phys. Rev. E. 56 (1997) 1346–1356.
[6] N.V. Sarlis, S.-R.G. Christopoulos, Natural time analysis of the centennial earthquake catalog, Chaos 22 (2012) 023123.
[7] D.L. Turcotte, B.D. Malamud, Earthquakes as a complex system, Internat. Geophys. 81 (2002) 209–227.
[8] H. Kanamori, E. Brodsky, The physics of earthquakes, Rep. Progr. Phys. 67 (2004) 1429–1496.
[9] S. Stein, M. Liu, E. Calais, Q. Li, Mid-continent earthquakes as a complex system, Seismol. Res. Lett. 80 (2009) 551–553.
[10] S. Lennartz, V.N. Livina, A. Bunde, S. Havlin, Long-term memory in earthquakes and the distribution of interoccurrence times, EPL 81 (2008) 69001.
[11] A.E.M. El-Misiery, E. Ahmed, On a fractional model for earthquakes, Appl. Math. Comput. 178 (2006) 207–211.
[12] L. Telesca, L. Toth, Analysis of temporal fluctuations in the 1880–1994 seismicity of Pannonian basin, Fluct. Noise Lett. 9 (2010) 157–165.
[13] B. Gutenberg, C.F. Richter, Frequency of earthquakes in California, Bull. Seismol. Soc. Am. 34 (1944) 185–188.
[14] K. Christensen, Z. Olami, Variation of the Gutenberg–Richter b values and nontrivial temporal correlations in a spring-block model for earthquakes, J. Geophys. Res. 97 (1992) 8729–8735.
[15] T. Utsu, Y. Ogata, R.S. Matsuura, The centenary of the Omori formula for a decay law of aftershock activity, J. Phys. Earth. 43 (1995) 1–33.
[16] F. Omori, On the aftershocks of earthquakes, J. Coll. Sci. Imp. Univ. Tokyo 7 (1894) 111–200.
[17] P.A. Reasenberg, L.M. Jones, Earthquake hazard after a mainshock in California, Science 243 (1989) 1173–1176.
[18] M. Lindman, B. Lund, R. Roberts, K. Jonsdottir, Physics of the Omori law: inferences from interevent time distributions and pore pressure diffusion modelling, Tectonophysics 424 (2006) 209–222.
[19] B.K. Chakrabarti, R.B. Stinchcombe, Stick-slip statistics for two fractal surfaces: a model for earthquakes, Physica A 270 (1999) 27–34.
[20] D. Yang, P. Yang, C. Zhang, Chaotic characteristic analysis of strong earthquake ground motions, Internat. J. Bifur. Chaos 22 (2012) 1250045.

[21] P.G. Okubo, K. Aki, Fractal geometry in the San Andreas fault system, J. Geophys. Res. 92 (1987) 345–355.
[22] A. Sornko, D. Sornette, Self-organized criticality and earthquakes, Europhys. Lett. 9 (1989) 197–202.
[23] S. Samko, A. Kilbas, O. Marichev, Fractional Integrals and Derivatives: Theory and Applications, Gordon and Breach Science Publishers, London, 1993.
[24] K. Miller, B. Ross, An Introduction to the Fractional Calculus and Fractional Differential Equations, John Wiley and Sons, New York, 1993.
[25] I. Podlubny, Fractional Differential Equations, Academic Press, San Diego, 1999.
[26] A. Kilbas, H.M. Srivastava, J. Trujillo, Theory and Applications of Fractional Differential Equations, Elsevier, Amsterdam, 2006.
[27] K. Diethelm, The Analysis of Fractional Differential Equations, Springer, Berlin, 2010.
[28] D. Baleanu, K. Diethelm, E. Scalas, J.J. Trujillo, Fractional Calculus: Models and Numerical Methods, in: Series on Complexity, Nonlinearity and Chaos, World Scientific Publishing, Singapore, 2012.
[29] M.D. Ortigueira, Fractional Calculus for Scientists and Engineers, Springer, Dordrecht, 2011.
[30] D. Baleanu, A. Golmankhaneh, A. Golmankhaneh, R. Nigmatullin, Newtonian law with memory, Nonlinear Dynam. 60 (2010) 81–86.
[31] C. Ionescu, J. Machado, R. De Keyser, Modeling of the lung impedance using a fractional order ladder network with constant phase elements, IEEE Trans. Biomed. Circuits Syst. 5 (2011) 83–89.
[32] E. Scalas, R. Gorenflo, F. Mainardi, Fractional calculus and continuous-time finance, Physica A 284 (2000) 376–384.
[33] F. Duarte, J. Machado, G. Duarte, Dynamics of the Dow Jones and the NASDAQ stock indexes, Nonlinear Dynam. 61 (2010) 691–705.
[34] C. Ionescu, P. Segers, R. De Keyser, Mechanical properties of the respiratory system derived from morphologic insight, IEEE Trans. Biomed. Eng. 56 (2009) 949–959.
[35] C. Ionescu, J. Tenreiro Machado, Mechanical properties and impedance model for the branching network of the sapping system in the leaf of Hydrangea Macrophylla, Nonlinear Dynam. 60 (2010) 207–216.
[36] J.A. Tenreiro Machado, António C. Costa, Maria Dulce Quelhas, Fractional dynamics in DNA, Commun. Nonlinear Sci. Numer. Simul. 16 (2011) 2963–2969.
[37] R.R. Nigmatullin, Fractional kinetic equations and universal decoupling of a memory function in mesoscale region, Physica A 363 (2006) 282–298.
[38] A. Oustaloup, X. Moreau, M. Nouillant, The CRONE suspension, Control Eng. Practice 4 (1996) 1101–1108.
[39] I. Petras, A note on the fractional-order Chua's system, Chaos Solitons Fractals 38 (2008) 140–147.
[40] H.L. Cao, Z.H. Deng, X. Li, J. Yang, Y. Qin, Dynamic modeling of electrical characteristics of solid oxide fuel cells using fractional derivatives, Int. J. Hydrog. Energy 35 (2010) 1749–1758.
[41] W. Dzwinel, D.A. Yuen, K. Boryczko, Y. Ben-Zion, S. Yoshioka, T. Ito, Nonlinear multidimensional scaling and visualization of earthquake clusters over space, time and feature space, Nonlinear Process. Geophys. 12 (2005) 117–128.
[42] International Seismological Centre, On-line Bulletin, Internatl Seis Cent, Thatcham, United Kingdom. http://www.isc.ac.uk, 2010 (accessed 02.04.2012).
[43] http://earthquake.usgs.gov/ (accessed 14.04.2012).
[44] J.B. Young, B.W. Presgrave, H. Aichele, D.A. Wiens, E.A. Flinn, The Flinn–Engdahl regionalisation scheme: the 1995 revision, Phys. Earth Planet. In. 96 (1996) 223–297.
[45] E.A. Flinn, E.R. Engdahl, A.R. Hill, Seismic and geographical regionalization, Bull. Seismol. Soc. Am. 64 (1974) 771–993.
[46] E.A. Flinn, E.R. Engdahl, A proposed basis for geographical and seismic regionalization, Rev. Geophys. 3 (1965) 123–149.
[47] J.A. Tenreiro Machado, G.M. Duarte, F.B. Duarte, Identifying economic periods and crisis using the multidimensional scaling, Nonlinear Dynam. 63 (2011) 611–622.
[48] A. Kilbas, H.M. Srivastava, J. Trujillo, Theory and Applications of Fractional Differential Equations, Elsevier, Amsterdam, 2006.
[49] K. Diethelm, The Analysis of Fractional Differential Equations, Springer, Berlin, 2010.
[50] W. Torgerson, Theory and Methods of Scaling, Wiley, New York, 1958.
[51] M. Bronstein, A. Bronstein, R. Kimmel, I. Yavneh, Multigrid multidimensional scaling, Numer. Linear Algebra Appl. 13 (2006) 149–171.
[52] I. Borg, P. Groenen, Modern Multidimensional Scaling Theory and Applications, second ed., Springer-Verlag, New York, 2005.
[53] J. Kruskal, Multidimensional scaling by optimizing goodness of fit to a nonmetric hypothesis, Psychometrika 29 (1964) 1–27.
[54] J.O. Ramsay, Some small sample results for maximum likelihood estimation in multidimensional scaling, Psychometrika 45 (1980) 139–144.
[55] J. Matheus, A. Dourado, J. Henriques, M. Antonio, D. Nogueira, Iterative multidimensional scaling for industrial process monitoring, in: IEEE International Conference on Systems, Man, and Cybernetics, Taipei, Taiwan, 2006.
[56] C. Tzagarakis, T.A. Jerde, S.M. Lewis, K. Ugurbil, A.P. Georgopoulos, Cerebral cortical mechanisms of copying geometrical shapes: a multidimensional scaling analysis of FMRI patterns of activation, J. Exp. Brain Res. 194 (2009) 369–380.
[57] J.A. Tenreiro Machado, F.B. Duarte, G.M. Duarte, Analysis of financial data series using fractional Fourier transform and multidimensional scaling, Nonlinear Dynam. 65 (2011) 235–245.
[58] J.A. Tenreiro Machado, A.C. Costa, M.F.M. Lima, Dynamical analysis of compositions, Nonlinear Dynam. 65 (2011) 399–412.
[59] C.M. Ionescu, J.A. Tenreiro Machado, R.D. Keyser, Is multidimensional scaling suitable for mapping the input respiratory impedance in subjects and patients? Comput. Methods Programs Biomed. 104 (2011) 189–200.
[60] X. Ji, H. Zha, Sensor positioning in wireless ad-hoc sensor networks using multidimensional scaling, in: Proc. IEEE INFOCOM, 2004.
[61] F.K.W. Chan, H.C. So, Efficient weighted multidimensional scaling for wireless sensor network localization, IEEE Trans. Signal Process. 57 (2009) 4548–4553.
[62] B. Ahrens, Distance in spatial interpolation of daily rain gauge data, Hydrol. Earth Syst. Sc. 10 (2006) 197–208.
[63] F.B. Duarte, J.A. Tenreiro Machado, G.M. Duarte, Dynamics of the Dow Jones and the Nasdaq stock indexes, Nonlinear Dynam. 61 (2010) 691–705.